

... (1.67 10⁵) ...
 ... 27 ...
 ... 29 ...
 ... L₂ ...
 ... H ...
 ... (IF) ...
 ... C₄ ...
 ... CC@C₄-C A ...
 ... (3D) ...
 ... C₄ ...
 ... L₂ ...
 ... /CC@C₄-C A ...
 ... 1121 ...
 ... 746 ...
 ... 500 ...
 ... 0.035% ...
 ... ≈ 100%.

2. Experimental

2.1. Preparation of CC@ZIF-67

C ... (CC 2 ... 2 ...)
 90 C ...
 (100 mL) ... C (...)₂ 6H₂ (0.72 g) ...
 (2-M I_{rr}, 1.64) ...
 ... CC@ IF-67 ...
 ... 60 C ...

2.2. Preparation of CC@Co₃O₄-PCNA and CC@Co₄N-PCNA

... CC@ IF-67 ...
 600 C ...
 330 C ...
 ... CC@C₃-C A ...
 ... CC@C₃-C A ...
 600 C ...
 fl H₃ (50 mL) ...
 ... CC@C₄-C A ...

2.3. Preparation of CC@PCNA, CC@Co₄N NWs, ZIF-67 and Co₄N-PC

CC@ IF-67 ... 600 C ...
 2 C ...
 ... (1M) ...
 ... CC@ C A ...
 ... CC@C₃-C A ...
 ... CC@C₃-C A ...
 ... CC@ ...
 ... C (...)₂ 6H₂ (0.41), H₄F (0.13) ...
 ... (0.42) ...
 ... H₃ ...
 ... CC ...
 ... 100 mL ...
 ... 120 C ...
 ... 60 C ...
 ... 330 C ...
 ... CC@C₃-C A ...
 ... CC@C₃-C A ...
 ... CC@C₄-C A ...

I_{rr} ... C (...)₂ 6H₂ (0.72g) ... 2-M I_{rr} ...
 (1.64g) ... (50 mL) A ...
 ... 4 ...
 ... 70 C ...
 ... IF-67 ...
 ... CC@C₄-C A ...

2.4. Preparation of the sulfur composites

/CC@C₄-C A, /CC@C₃-C A, /CC@C₄-C A ...
 /CC@C₄-C A, /CC@C₃-C A, /CC@C₄-C A ...
 50 ...
 (0.15) ... C₂ (10 mL) D y CC@C₄-C A ...
 ... C₂ ...
 ... 50 C ...
 ... CC@C₄-C A ...
 ... 155 C ...
 ... 12 (F . 1) ...
 C₃-C A, /CC@C₄-C A, /CC@C₃-C A, /CC@C₄-C A ...
 1.01–6.20 ...

2.5. Preparation of the Li₂S₆ solution

L₂ ... 1:5 ...
 ... (HF) ...

2.6. Material characterization

... FE-EM (... 55), EM (JEM-2000B), H -
 EM (G2 20), (E CALAB 250, A-Kα ...), D
 (D/MAP-2400, C Kα ...), (DF ...), IC
 (E I 300D), E ... (EL III),
 GA (D G-60AH) ... (A L200B) ...

2.7. Electrochemical measurement

F ...
 2025 ...
 0.1 mL ...
 ... 1.0 M L F I ...
 D L/DME (1:1 y ...; F I = (fl ...) ...
 D L = 1,3- ... DME = ... 2.0 % L₃ ...
 ... 45 μL ...
 C 2001A ... 1.7 ... 2.8 ...
 ... (C) ... I_{rr} ...
 (EI) ... 1.7 ... 2.8 ... 0.1 ...

2.8. Density functional theory calculations

... y (DF) ...
 ... (A) 51,52 ...
 ... 53 ...
 ... 54 ...
 ... y. A ... 500 ...
 ... F ...
 ... 0.05 ... B ...
 ... 5 5 1 - ... 55 . A ...
 fl - y ...

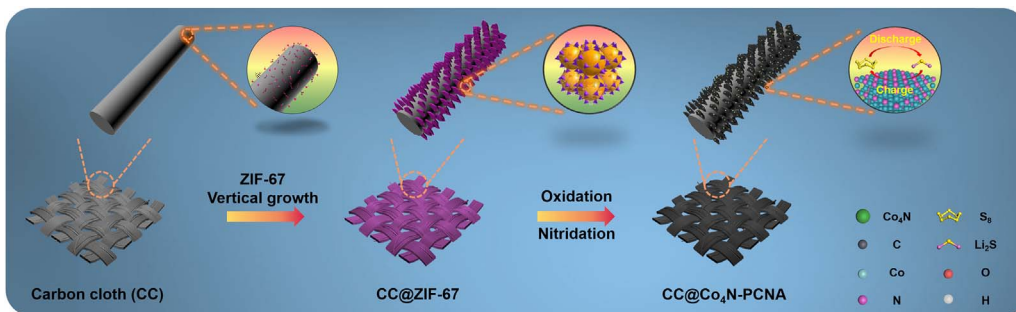


Fig. 1. Schematic diagram of the synthesis process for CC@Co₄N-PCNA.

$$E_b = E_{Li_2S_n} + E_{Co_4N} - E_{Li_2S_n + Co_4N} \quad (1)$$

3. Results and discussion

Figure 1 shows the synthesis process for CC@Co₄N-PCNA. The process starts with carbon cloth (CC) and ZIF-67. ZIF-67 is grown vertically on the CC surface. The resulting CC@ZIF-67 is then subjected to oxidation and nitridation to form CC@Co₄N-PCNA. The legend identifies the components: Co₄N (green circle), C (grey circle), Co (blue circle), N (purple circle), S₈ (yellow star), and Li₂S (red circle).

The synthesis process for CC@Co₄N-PCNA involves the vertical growth of ZIF-67 on carbon cloth (CC) to form CC@ZIF-67, followed by oxidation and nitridation to form CC@Co₄N-PCNA. The legend identifies the components: Co₄N (green circle), C (grey circle), Co (blue circle), N (purple circle), S₈ (yellow star), and Li₂S (red circle).

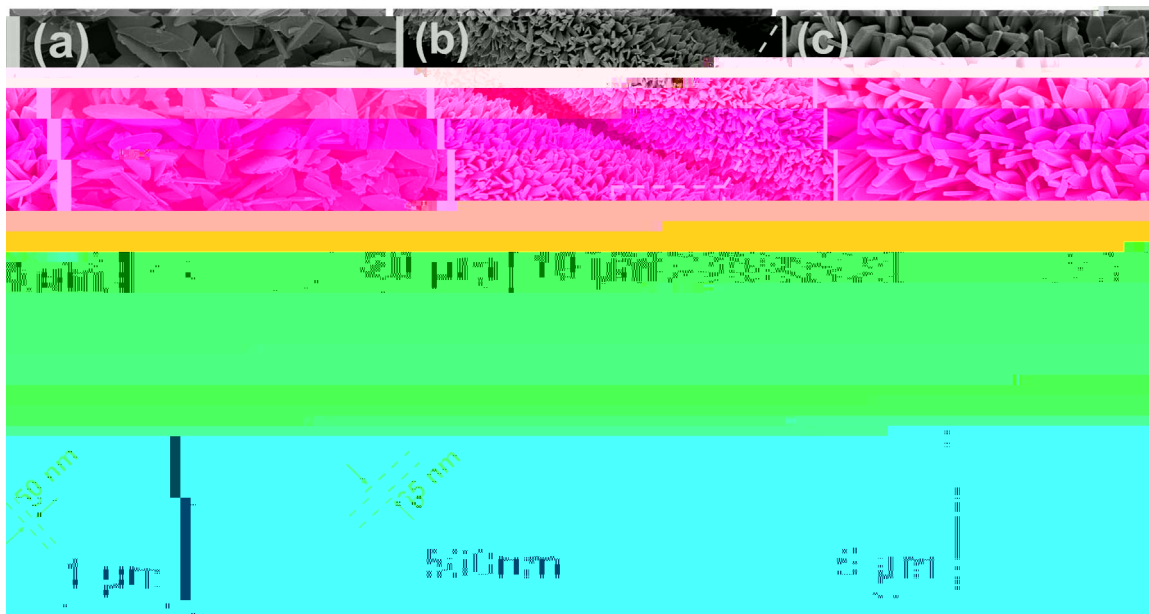


Fig. 2. FE-EM images of (a) IF-67, (b) CC@IF-67, (c) CC@C₃₄-C A, and (d) CC@C₄-C A.

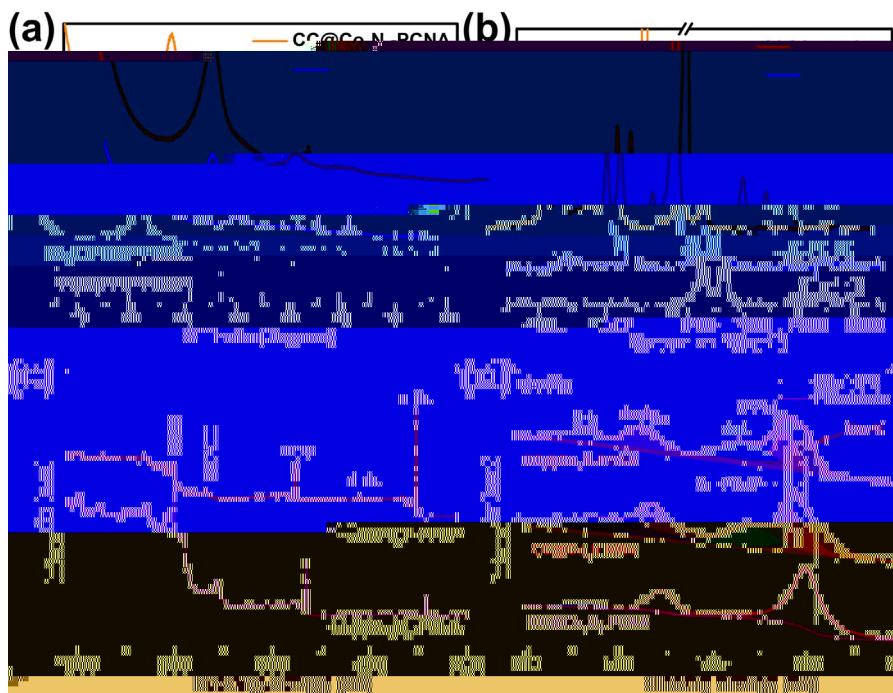


Fig. 4. (a) XRD patterns of CC@Co-Ni-BCNA and (b) XRD patterns of CC@C4. The inset shows the enlarged view of the (001) and (002) peaks. The x-axis is 2θ (°) and the y-axis is Intensity (a.u.).

The electrochemical performance of the synthesized materials was evaluated by cyclic voltammetry (CV) and galvanostatic charge-discharge (GCD) tests. The CV curves of CC@Co-Ni-BCNA and CC@C4 in 0.1 M NaOH at various scan rates (5, 10, 20, 50, 100, 200, 500, 1000 mV s⁻¹) are shown in Fig. 5(a). The redox peaks corresponding to the redox reactions of the active materials are clearly observed. The area under the CV curves was integrated to obtain the GCD curves, as shown in Fig. 5(b). The discharge curves show a typical rectangular shape, indicating good capacitive behavior. The specific capacitance (C_s) was calculated using the equation: $C_s = \frac{Q}{m \cdot \Delta V}$, where Q is the discharge charge, m is the mass of the active material, and ΔV is the potential window. The C_s values for CC@Co-Ni-BCNA and CC@C4 are listed in Table 1. The C_s values increase with increasing scan rate, which is characteristic of pseudocapacitive behavior. The Ragone plot in Fig. 5(c) shows the power density (P) versus energy density (E) for both materials. The CC@Co-Ni-BCNA material exhibits a higher power density compared to CC@C4, indicating better rate capability. The electrochemical impedance spectroscopy (EIS) spectra were recorded at various frequencies (0.01, 0.1, 1, 10, 100, 1000, 10000 Hz) and are shown in Fig. 5(d). The Nyquist plots show a semicircle at high frequencies and a linear region at low frequencies, indicating a combination of capacitive and resistive processes. The equivalent circuit model (ECM) is shown in Fig. 5(e), consisting of a series combination of a resistor (R_s) and a constant phase element (CPE). The R_s values for CC@Co-Ni-BCNA and CC@C4 are 1.7 Ω and 2.8 Ω, respectively. The CPE values are 0.5 C and 0.2 C, respectively. The Nyquist plots also show the presence of a Warburg impedance element (W) at low frequencies, indicating diffusion-controlled processes. The EIS spectra were fitted with the ECM using the software ZView. The fitting parameters are listed in Table 2. The R_s values are 1.7 Ω and 2.8 Ω, and the CPE values are 0.5 C and 0.2 C. The Warburg impedance (W) values are 170 Ω and 190 Ω, respectively. The EIS spectra were recorded at various frequencies (0.01, 0.1, 1, 10, 100, 1000, 10000 Hz) and are shown in Fig. 5(d). The Nyquist plots show a semicircle at high frequencies and a linear region at low frequencies, indicating a combination of capacitive and resistive processes. The equivalent circuit model (ECM) is shown in Fig. 5(e), consisting of a series combination of a resistor (R_s) and a constant phase element (CPE). The R_s values for CC@Co-Ni-BCNA and CC@C4 are 1.7 Ω and 2.8 Ω, respectively. The CPE values are 0.5 C and 0.2 C, respectively. The Warburg impedance (W) values are 170 Ω and 190 Ω, respectively.

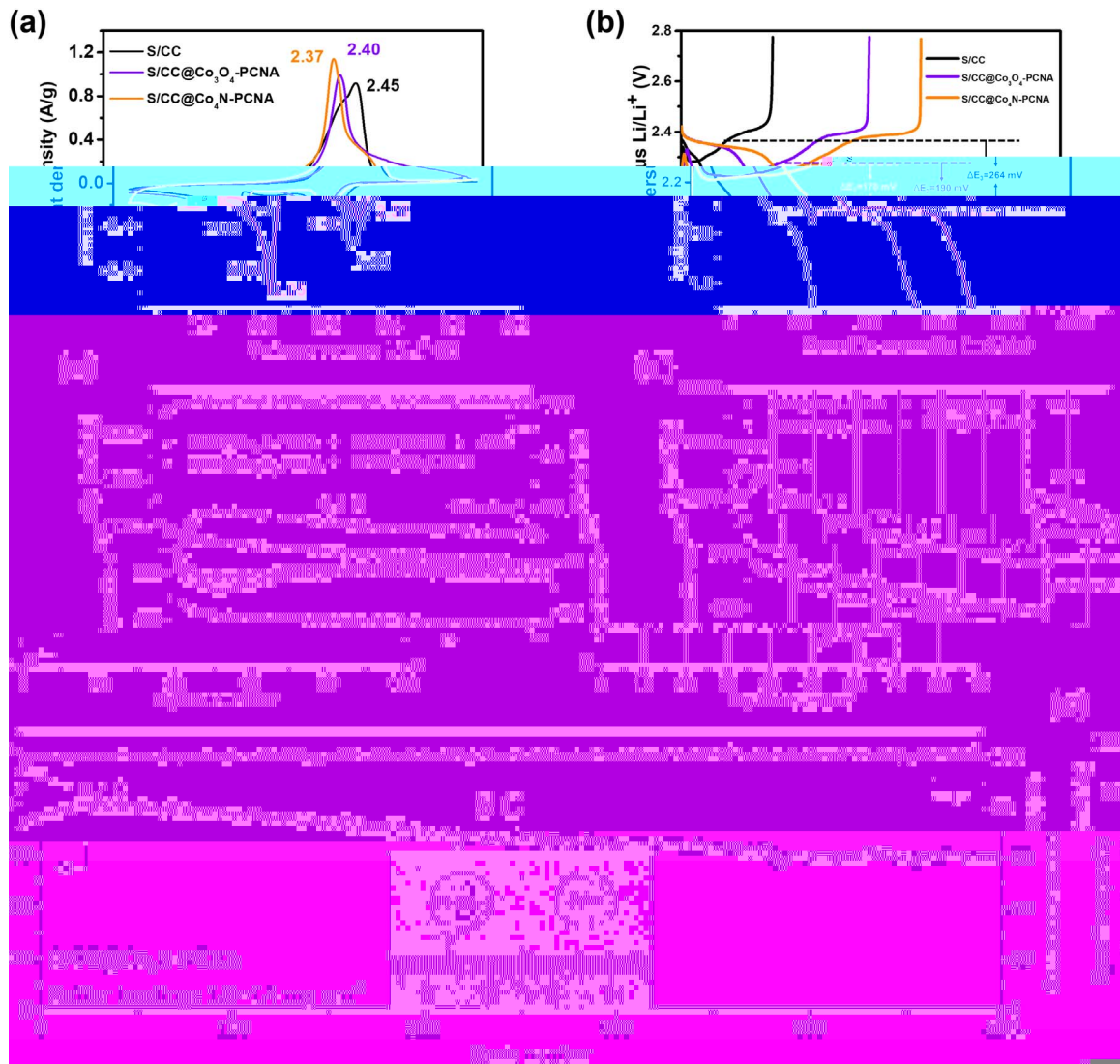


Fig. 5. (a) Cyclic voltammetry (CV) curves of S/CC, S/CC@Co₃O₄-PCNA, and S/CC@Co₄N-PCNA at various scan rates (0.2 C, 0.5 C, 1 C, 2 C, 5 C, 10 C, 20 C, 50 C, 100 C). The inset shows the magnified view of the peaks at 2.37, 2.40, and 2.45 V. (b) Charge-discharge curves of S/CC, S/CC@Co₃O₄-PCNA, and S/CC@Co₄N-PCNA at 0.5 C. The potential window is from 2.2 to 2.8 V. The voltage drop (ΔE₀) is 264 mV. The inset shows the magnified view of the curves near 2.2 V.

3D surface plots of the CV curves are shown below the plots, illustrating the changes in the electrochemical response of the materials at different scan rates. The schematic diagram shows the layered structure of the electrode, consisting of S/CC, S/CC@Co₃O₄-PCNA, and S/CC@Co₄N-PCNA layers.

Electrochemical Impedance Spectroscopy (EIS) Nyquist plots are also shown, indicating the charge transfer resistance (R_{ct}) and the Warburg impedance (Z_w) for the materials. The equivalent circuit model used for fitting the EIS data is shown in the inset, consisting of a series combination of a resistor (R_s) and a parallel combination of a resistor (R_{ct}) and a constant phase element (CPE).

The Nyquist plots show the Nyquist impedance (Z_N) vs. the negative imaginary impedance (-Z_i). The R_{ct} values for S/CC, S/CC@Co₃O₄-PCNA, and S/CC@Co₄N-PCNA are 55.6 Ω, 56.4 Ω, and 56.3 Ω, respectively. The Warburg impedance (Z_w) values are 0.7 Ω, 0.7 Ω, and 0.7 Ω, respectively. The total impedance (Z_{total}) values are 778.5 Ω, 796.7 Ω, and 781.3 Ω, respectively.

The EIS results indicate that the S/CC@Co₃O₄-PCNA and S/CC@Co₄N-PCNA materials exhibit lower R_{ct} and Z_w values compared to S/CC, suggesting improved electrochemical kinetics and ion transport. The total impedance (Z_{total}) values are also lower for the PCNA-coated materials, indicating better overall electrochemical performance.

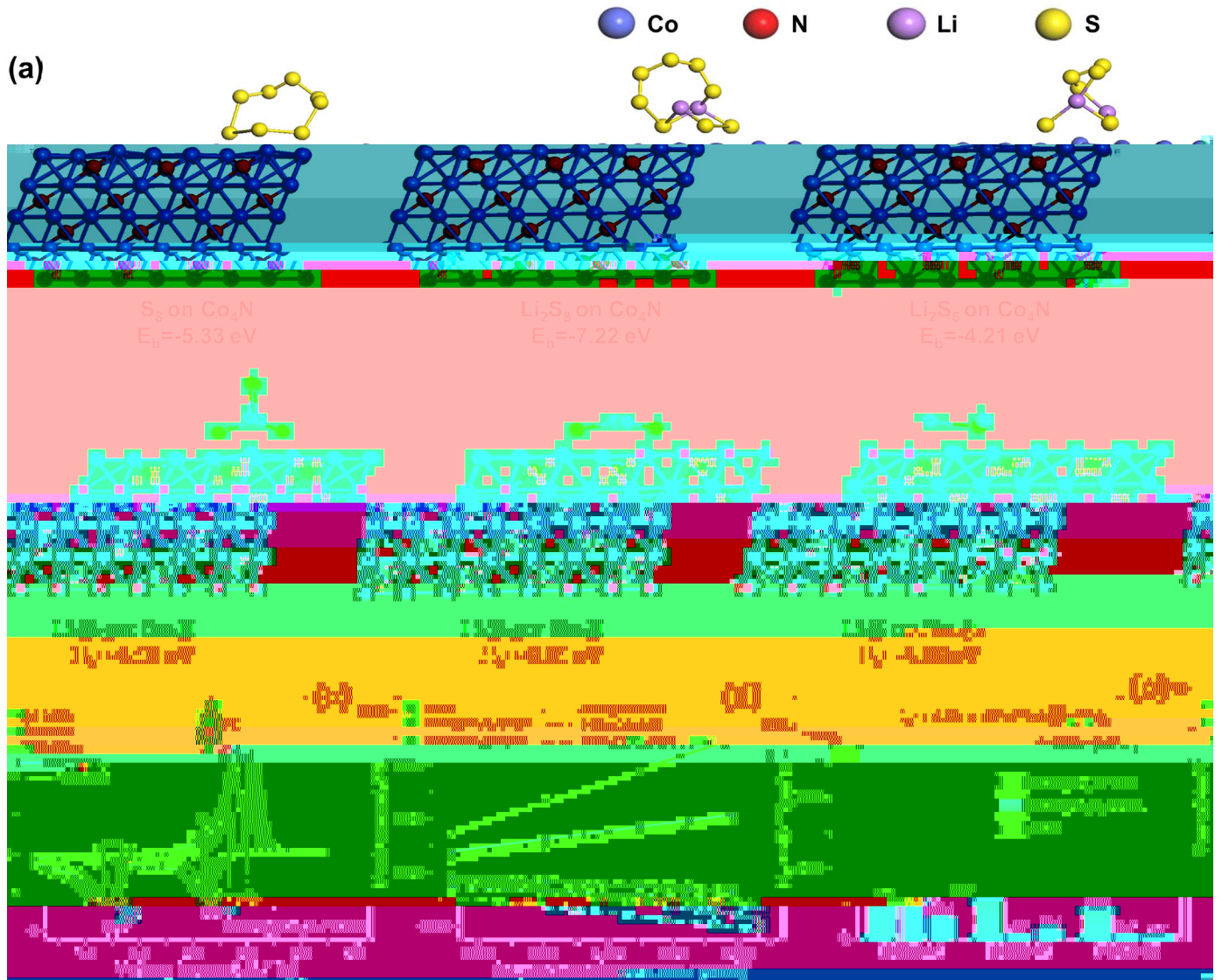


Fig. 6. (a) S₈ on Co₂N and Li₂S₈ on Co₂N. (b) Charge density difference isosurfaces. (c) Band structure plots.

$I_p = 2.69 \times 10^5 n^{0.5} a D_{Li^+}^{0.5} v^{0.5} C_{Li}$ (3)

The electrochemical performance of the Co₂N-based electrodes was evaluated by cyclic voltammetry (CV) and galvanostatic charge-discharge (GCD) tests. The CV curves show a typical redox couple for the S₈/Li₂S₈ system. The GCD curves show a long discharge plateau at approximately 1.7 V, indicating a high capacity. The rate capability of the electrodes was tested at various current densities, showing a stable performance even at high rates. The cycling stability was also evaluated, showing a high capacity retention over multiple cycles.

The electrochemical impedance spectroscopy (EIS) spectra were recorded to investigate the charge transfer kinetics. The Nyquist plots show a semicircle at high frequencies, corresponding to the charge transfer resistance (R_{ct}). The equivalent circuit model was fitted to the experimental data, and the R_{ct} values were determined. The R_{ct} values for the Co₂N/S₈ and Co₂N/Li₂S₈ electrodes are 23.48 Ω and 15.41 Ω, respectively, indicating a low charge transfer resistance and fast electrochemical kinetics.

The diffusion coefficients (D) of Li⁺ ions in the electrodes were calculated using the Randles-Sevcik equation. The D values for the Co₂N/S₈ and Co₂N/Li₂S₈ electrodes are 4.1 × 10⁻¹⁴ cm² s⁻¹ and 2.7 × 10⁻¹³ cm² s⁻¹, respectively. The calculated D values are in good agreement with the experimental results, indicating a fast diffusion of Li⁺ ions in the electrodes.

The electrochemical performance of the Co₂N-based electrodes was compared with other reported S₈/Li₂S₈ systems. The Co₂N-based electrodes show a higher capacity and better rate capability than other reported systems. This is attributed to the unique structure of Co₂N, which provides a large surface area and a high density of active sites for the electrochemical reactions.

fi y . , C₄ ff ” L ” y ”
 ff ” y fi ” y . I ” ,
 ” y ” y ” -1 660 - ” -1, y (” F . 21,
 ” 5), ”
 L B ” - ” - ” , ” ”

4. Conclusions

I ” ” y, ” ” C₄ ” ” ”
 ” ” ” L B . ” ” ”
 C₄ ” ” ” ff ” ” L ” ff ”
 ” ” ” y fi . B ” fi ”
 ” ” y ff ” ” L ” y CC@
 C₄ - C A, /CC@C₄ - C A ” ”
 y 1121 ” A⁻¹ 0.5 C 100 y , ” ”
 y 746 ” A⁻¹ 5 C ” y
 0.035% y 500 y 5 C. ” ” ”
 ” ” ” ” ” ” y ” -
 ” ” fl ” ” ” ” ” ”

Acknowledgment

C ” (G ” . 51672033, -1610105, -1610255), F ” F ”
 K y L ” y I ” ” E ” ” A ”
 M ” , M ” y E ” C ” (KLI EAM 201601), ” ”
 ” ” F ” L E ” ” ” , D ”
 - ” y ” y, C ” (2016-54).

Appendix A. Supporting information

” ” y
 ” ” ” :10.1016/ . ” ” 2018.12.005 ” ” ”

References

- 1 .G.B . , A.F ” , L.J.H . , J.M. ” L - 2 ” -
 ” y ” , . M . 11 (2011) 19–29.
- 2 . - ” , - ” , J.J.C . G. ” , . ” , M. . M D , . C H , . C ,
 ” - 2 y - ” ” . C ” ” 4 (2013) 1331.
- 3

9 (2017) 29881–29888.

26 M. B. C. H., H. H. B. J., *Energy Storage Materials* 20 (2017) 425–451.

27 C. K., L. L., F. C., J. C., *Energy Storage Materials* 3 (2016) 236–242.

28 L. B., B., C., J. J., *Energy Storage Materials* 2 (2017) 869–876.

29 D. D., F., J. J., J. C., C. D. B., M., F. D., *Energy Storage Materials* 11 (2017) 6031–6039.

30 K., K., J., H. C., C. K., J., J., H. By., H. M. L., I. D. K., B., *Energy Storage Materials* 12 (2018) 128–139.

31 M. D. M., M., H., G., *Energy Storage Materials* 5 (2017) 2972–2980.

32 F. L., J. L., B., L., *Energy Storage Materials* 302 (2016) 174–179.

33 G., C., L., J., L., C., H. H., M., H., *Energy Storage Materials* (2017) 1701288.

34 L., J. L., G., F., B. L., B. L., F. K., H., *Energy Storage Materials* 10 (2017) 1694–1703.

35 G. L., M., A. C., C. J., L., J., H., J. L., *Energy Storage Materials* 12 (2018) 6013–6022.

36 C. L., D., G., L., C., L., C., /M F - $A_2(H)_{2.76}F_{3.24}$, *Energy Storage Materials* 12 (2018) 341–351.

37 D., J., H., J. C., A., *Energy Storage Materials* 12 (2018) 2381–2388.

38 H., H., M., J., H., H., / *Energy Storage Materials* 28 (2018) 1707536.

39 L. L., L., J. L., C., F., K. A., *Energy Storage Materials* 262 (2014) 380–385.

40 M. H. y., M., *Energy Storage Materials* 189 (2009) 416–422.

41 B., y., H. J. F., *Energy Storage Materials* 4 (2016) 17801–17808.

42 L., J., C. J. C., L., J. M., *Energy Storage Materials* A 2 (2014) 12177–12184.

43 J., C., H. F., D., G., M., *Energy Storage Materials* A 6 (2018) 2797–2807.

44 L., C., J. H., C., H., C., L., J., *Energy Storage Materials* 7 (2017) 1601843.

45 L. M., C., G., H., C., J. L., J., C., *Energy Storage Materials* 11 (2017) 7274–7283.

46 D. K., L. F., A., *Energy Storage Materials* 3 (2016) 130–136.

47 L., J., B. G., D., L. M. L., A., *Energy Storage Materials* 7 (2016) 13065.

48 L., J., M., J., C., *Energy Storage Materials* 13 (2017) 1701013.

49 J., C. L., H., G., C., B., *Energy Storage Materials* 7 (2016) 11203.

50 J., K., L., L. F., A., *Energy Storage Materials* 8 (2009) 500–506.

51 G. K., J. H., A., *Energy Storage Materials* B 48 (1993) 13115–13118.

52 G. K., J. F., *Energy Storage Materials* B 54 (1996) 11169–11186.

53 E. B., *Energy Storage Materials* B 50 (1994) 17953–17979.

54 J., A., *Energy Storage Materials* B 45 (1992) 13244–13249.

55 H. J. M., J. D., *Energy Storage Materials* B 13 (1976) 5188–5192.

56 G., H., J., B. L., D., L., J., *Energy Storage Materials* L 2 (2017) 840–845.

57 J., H. F., F. C., D., G., *Energy Storage Materials* 51 (2018) 73–82.